GEOLOGY | THE GEOLOGICAL SOCIETY OF AMERICA®

https://doi.org/10.1130/G49566.1

Manuscript received 8 June 2021
Revised manuscript received 7 August 2021
Manuscript accepted 29 September 2021

Published online 22 November 2021

Water in omphacite fingerprints the thermal history of eclogites

Peilin Jiang[1], Hanyong Liu[1], Henrik Skogby[2], Ren-Xu Chen[3] and Xiaozhi Yang[1]*

[1]State Key Laboratory for Mineral Deposits Research, School of Earth Sciences and Engineering, Nanjing University, Nanjing 210023, China

[2]Department of Geosciences, Swedish Museum of Natural History, Box 50007, 104 05 Stockholm, Sweden

[3]Chinese Academy of Sciences Key Laboratory of Crust-Mantle Materials and Environments, School of Earth and Space Sciences, University of Science and Technology of China, Hefei 230026, China

ABSTRACT

Omphacite is a diagnostic mineral of high- and ultrahigh-pressure rocks, and its association with garnet is characteristic of eclogites from subduction-related massifs and volcano-entrained xenoliths. Omphacite can accommodate significant amounts of water as structurally bound hydroxyl (OH) groups, and is able to convey water into Earth's interior. We show, for the first time, experimental evidence that the infrared absorption patterns of water in omphacite are temperature sensitive. This provides a new framework for discriminating water in natural omphacite equilibrated at different temperatures. We also demonstrate that in low-temperature omphacite, the integral absorbance ratio between the infrared OH absorption bands at 3620 cm^{-1} and 3450 cm^{-1} is linearly related to temperature. Water in omphacite of massif eclogites records the temperature of OH equilibrium, allowing reconstruction of the fluid-involved thermal history and tectonics of rock evolution.

INTRODUCTION

In the past few decades, water in nominally anhydrous minerals (NAMs) has received intense attention as a result of studies on natural and synthetic samples. Although present at parts-per-million (ppm) levels in NAMs, water has a disproportionate effect on many physical and chemical properties of the host minerals, and on Earth's dynamics. Typically, water lowers melting temperature (Hirose and Kawamoto, 1995; Gaetani and Grove, 1998), promotes ionic diffusion (Hier-Majumder et al., 2005; Costa and Chakraborty, 2008), facilitates plastic deformation (Mackwell et al., 1985; Mei and Kohlstedt, 2000), and enhances electrical conductivity (Karato, 1990; Yang et al., 2011; Yang and McCammon, 2012; Zhang et al., 2012; Liu et al., 2021). Therefore, water in NAMs is key to understanding processes of the deep Earth.

Water chiefly occurs as OH groups in NAMs, though molecular hydrogen (H_2) can also be structurally present (Yang et al., 2016; Moine et al., 2020). Omphacite [$(Ca,Na)(Mg,Fe^{2+},Al)Si_2O_6$] is unique among NAMs in the crust and upper mantle because of its high OH content of as much as >1500 ppm H_2O (Skogby et al., 1990; Smyth et al., 1991; Katayama and Nakashima, 2003). Omphacite is typical of eclogite, an important rock in subducted slabs and in local areas in the upper mantle as indicated by various massif and xenolith eclogites. Omphacite can transport water to Earth's interior, and its OH storage is crucial for insights into the deep water cycle. The patterns of infrared OH absorption bands in omphacite, differing from those of other clinopyroxenes such as augite and diopside, vary greatly between different samples and between different zones at subgrain scales (Skogby et al., 1990; Smyth et al., 1991; Katayama and Nakashima, 2003; Koch-Müller et al., 2004; Sheng et al., 2007; Schmädicke and Gose, 2017). However, the reason for the diversity of OH bands and the implications are not well understood. We show experimentally that the infrared OH patterns of omphacite are temperature dependent.

EXPERIMENTS AND METHODS

Our starting sample was a massif eclogite from Bixiling (Dabie Shan, China), consisting of omphacite, garnet, and <3% quartz and rutile. Omphacite grains, 0.3–0.9 mm in size and chemically uniform (Table S1 in the Supplemental Material[1]), were handpicked from crushed eclogite; initial OH content was 180 ppm H_2O (Fig. S1). Grains were loaded, along with eclogite powder, NiO, and 2–3 wt% distilled water, into thick-walled Ni capsules (inner diameter 4.2 mm, outer diameter 5 mm, and length 10 mm; Yang, 2015, 2016; Liu and Yang, 2020) and were annealed at 1–3 GPa and 600–1100 °C in a piston cylinder press with temperature measured by a type S thermocouple. The temperature gradient over the sample length was <25 °C (Bromiley et al., 2004). An extra run was done at 1 GPa and 700 °C in a Fe capsule with FeO (Fe-FeO [iron-wüstite] oxygen buffer [IW], ~5 log units more reducing than the Ni-NiO [NNO] oxygen buffer). Capsules were sealed by compression in the press. Duration was 36–310 h depending on temperature, and longer runs at otherwise the same conditions were also carried out (Table 1). Following previous work (Kohlstedt et al., 1996; Bromiley et al., 2004; Yang, 2015, 2016; Liu and Yang, 2020), sample chemistry was maintained so that the nonchemical effect on OH incorporation could be assessed. In particular, this is meaningful for massif eclogites because their mineral composition at peak metamorphism can be retained during exhumation. A retrogression run was done by re-annealing omphacite from the 1100 °C run at 800 °C (3 GPa). At the end of each run, the sample was quenched by switching off the power to the heating circuit, and pressure was then released. Recovered capsules were tested for the presence of excess water, and NNO or IW was confirmed to be present.

We analyzed recovered omphacite grains, commonly fractured, using a JEOL JXA-8230 electron microprobe and a Renishaw RM2000 Raman spectrometer. Fourier transform infrared (FTIR) spectra were measured using a Bruker Vertex 70 V spectrometer and a Hyperion 2000

*E-mail: xzyang@nju.edu.cn

[1]Supplemental Material. Fourier transform infrared and Raman spectra, electron microprobe data, and resolved band absorbance ratios of samples. Please visit https://doi.org/10.1130/GEOL.S.16942762 to access the supplemental material, and contact editing@geosociety.org with any questions.

CITATION: Jiang, P., et al., 2022, Water in omphacite fingerprints the thermal history of eclogites: Geology, v. 50, p. 316–320, https://doi.org/10.1130/G49566.1

TABLE 1. SUMMARY OF EXPERIMENTAL CONDITIONS AND WATER CONTENT

Run number	*P* (GPa)	*T* (°C)	O buffer	Duration (h)	H_2O (ppm)
B137	1	600	Ni-NiO	180	142
A157	1	600	Ni-NiO	310	153
A113	1	650	Ni-NiO	137	169
A115	1	700	Ni-NiO	134	200
A158	1	700	Ni-NiO	236	202
B219	1	700	Fe-FeO	141	284
B157	1	750	Ni-NiO	103	208
B148	1	800	Ni-NiO	90	710
B160	1	900	Ni-NiO	72	1144
B163	1	1000	Ni-NiO	41	1076
A133	2	700	Ni-NiO	136	225
A145	2	750	Ni-NiO	110	250
A147	2	800	Ni-NiO	92	277
A149	2	850	Ni-NiO	84	305
A150	2	900	Ni-NiO	71	1250
A154	2	1000	Ni-NiO	48	1719
B209	3	700	Ni-NiO	134	236
A148	3	750	Ni-NiO	111	287
B210	3	800	Ni-NiO	96	309
B215	3	900	Ni-NiO	71	325
A159	3	950	Ni-NiO	62	1303
A153	3	1000	Ni-NiO	45	1474
A155	3	1100	Ni-NiO	36	1688
B328*	3	800	Ni-NiO	90	340

Note: P—pressure; *T*—temperature.
*Retrogression run (B328, by reannealing grains of A155). Recovered grains are fragile and only two small grains (90-160 μm in size prior to polishing) are analyzed.

microscope. Samples were preheated at 150–200 °C, and inclusion- and crack-free areas were analyzed. Unpolarized spectra were taken on ≥10 randomly oriented grains in each sample due to the difficulty in preparing small grains for polarized work. Baseline corrections were applied via a spline fit of the spectra. Spectra of each sample were averaged, and water content was obtained from the absorption of OH bands at 3800–3000 cm^{-1} using the OH calibration for omphacite (Katayama et al., 2006) [$(8.34 \pm 1.46) \times 10^4$ L/mol/cm^2], and a correction factor of 3 (Kovács et al., 2008). Uncertainty is <20% except for the retrogression run (30%–50% or larger) for which only two grains were analyzed. Relative variation in water content is determined by the integral absorbance, and general results are not affected by the OH calibration. We resolved OH bands into Gaussian components with PeakFit software (http://sigmaplot.co.uk/products/peakfit/peakfit.php).

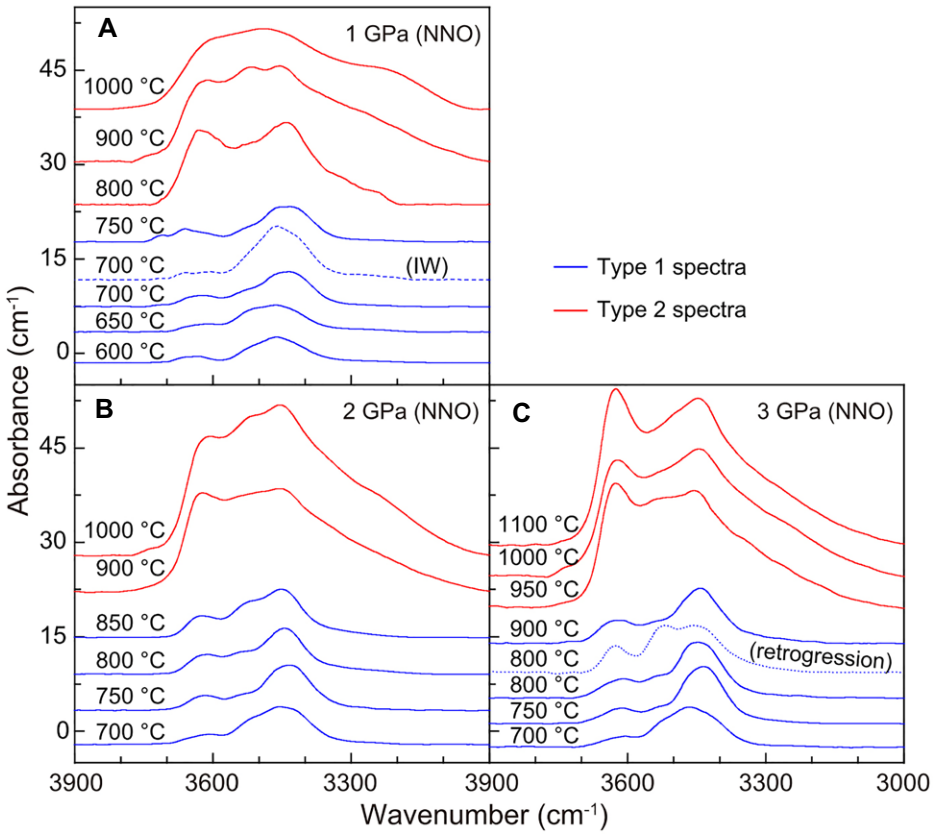

Figure 1. Average unpolarized Fourier transform infrared spectra of annealed omphacite from Bixiling (Dabie Shan, China). Pressure and temperature values indicate annealing conditions for each experiment. Solid line is with Ni-NiO (NNO) buffer; dashed line is with Fe-FeO (IW) buffer; dotted line is retrogression run (see text).

RESULTS

Annealed samples demonstrate no zoned distribution, with composition nearly the same as that of the starting mineral (Table S1). FTIR spectra show main absorption bands at ~3620, 3520, and 3450 cm^{-1} (Fig. 1). Positions and shapes of the bands resemble those previously reported for OH in omphacite (Skogby et al., 1990; Smyth et al., 1991; Katayama and Nakashima, 2003; Koch-Müller et al., 2004; Sheng et al., 2007; Schmädicke and Gose, 2017). Some weak bands at >3650 cm^{-1} and <3400 cm^{-1} are likely due to interference fringes or moisture variations in air, and their contribution to bulk water content is minor (notably, the integral absorbance of the main bands, as discussed below, is unaffected). Koch-Müller et al. (2004) assigned the strong bands at >3600 cm^{-1} in natural omphacite, as observed in our runs at 800–1100 °C (depending on pressure), to chlorite inclusions. However, chlorite is stable only at <700 °C (Schmidt and Poli, 2014), and hence these bands are most probably intrinsic in our samples. Profile analyses show similar OH absorption at subgrain scales, and OH patterns and contents are comparable at different durations (Figs. S2 and S3; Table 1), demonstrating OH equilibrium at the sample composition. In each run, OH bands are similar between different grains, though the relative intensities vary due to different orientations (Fig. S4). At given conditions, OH patterns (not contents) are similar using either the NNO or IW buffer, implying a minor redox effect, as reported also for other pyroxenes (Liu and Yang, 2020).

The OH bands differ between contrasting run temperatures (Fig. 1). At low temperature, the spectra show a strong band at 3450 cm^{-1} and a weak one at 3620 cm^{-1}, and the latter is enhanced by increasing temperature (type 1 spectra). At high temperature, the spectra show broad and intense bands at similar positions, and the intensity of the band at 3620 cm^{-1} is close to that at 3450 cm^{-1} (type 2 spectra). The transition from type 1 to type 2 spectra depends on pressure and temperature, e.g., 750–800 °C at 1 GPa and 900–950 °C at 3 GPa, and the transition curve is steeper at 1–2 GPa than at higher pressure (Fig. 2A). Type 1 spectra are restored by reannealing a high-temperature sample, showing type 2 spectra, at a low temperature in the retrogression run (Fig. 1C). For type 1 spectra, the average integral absorbance ratio between the bands at 3620 and 3450 cm^{-1}, Abs_{3620}/Abs_{3450}, is,

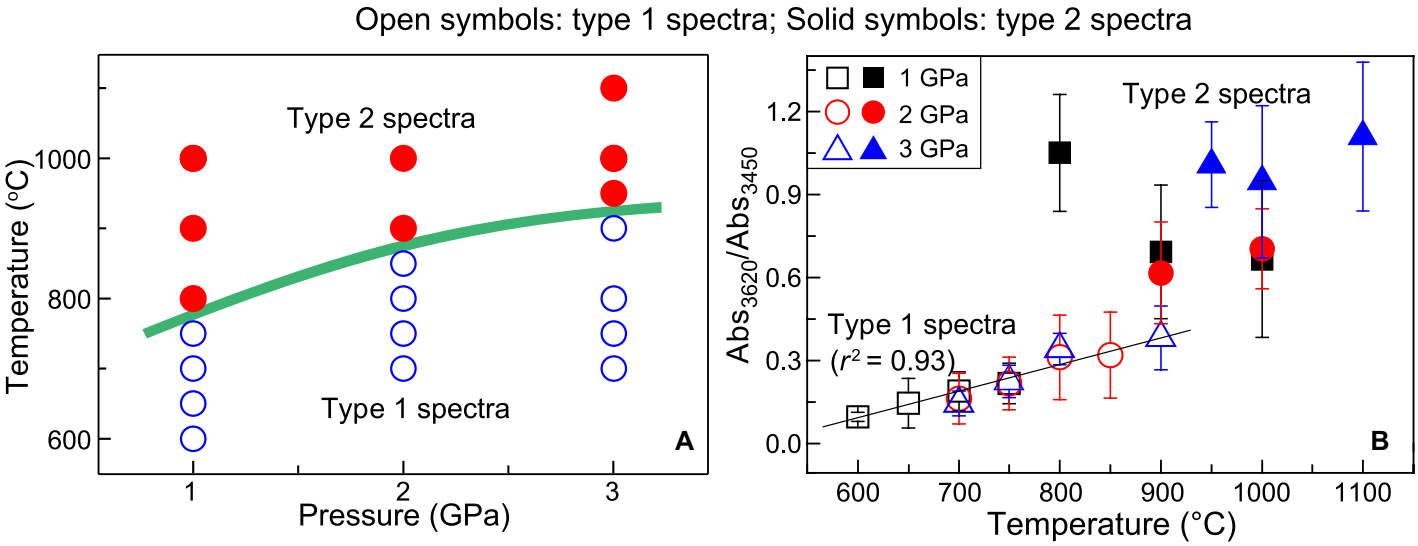

Figure 2. (A) Pressure and temperature conditions of type 1 and 2 spectra. Green curve indicates spectral transition. (B) Average integral absorbance ratio between bands at 3620 and 3450 cm^{-1} (Abs_{3620}/Abs_{3450}) versus temperature for various pressure conditions. Error bars are the standard deviation by averaging multiple grains (Table S2 [see footnote 1]). Solid line is the fit to data for type 1 spectra (Equation 1).

though independent of pressure, linearly related to temperature (T), a relationship that is absent for type 2 spectra (Fig. 2B):

$$Abs_{3620} / Abs_{3450} = (-0.48 \pm 0.06) + (9.55 \pm 0.85) \times 10^{-4} \times T. \quad (1)$$

Water content of annealed samples, e.g., the solubility of OH at water-saturated conditions, broadly increases with temperature and pressure (Table 1), in agreement with reported trends for other pyroxenes (Liu and Yang, 2020), but differs between samples showing type 1 (142–325 ppm) versus type 2 (710–1688 ppm) spectra.

CATION DISORDER AND OH INCORPORATION IN OMPHACITE

The OH incorporation in omphacite is charge balanced by cations and vacancies in the crystal lattice (Skogby et al., 1990; Smyth et al., 1991; Katayama and Nakashima, 2003). The studied samples show no change in chemistry and structure nor phase transition during the experiment (Table S1; Fig. S5). Thus, the variation in OH bands with temperature, as shown in Figures 1 and 2, is indicative of change in the types and populations of OH defects and/or cation arrangements, which are temperature sensitive. Omphacite is a solid solution of jadeite ($NaAlSi_2O_6$) and diopside ($CaMgSi_2O_6$), but its composition is complex due to other components such as Fe^{2+} as hedenbergite ($CaFe^{2+}Si_2O_6$) and Fe^{3+} as aegirine ($NaFe^{3+}Si_2O_6$). Jadeite and diopside have the $C2/c$ space group, with an octahedral M1 site and a polyhedral M2 site. This space group has disordered cations within the M1 and M2 sites. However, the space group of omphacite is different. At low temperature, the cations are ordered, e.g., by ordering of Mg, Al, and Fe on the M1 site and coupled ordering of Na and Ca on the M2 site. This results in a lower symmetry with the $P2/n$ space group (Fleet et al., 1978). As temperature increases, the cations are redistributed and the coupled ordering changes gradually. If a critical temperature is reached, the cations are largely disordered, and the space group is $C2/c$. The cation disorder can be retained if a crystal undergoes rapid cooling (Fleet et al., 1978; Katerinopoulou et al., 2008).

We suggest that changes in the patterns of type 1 versus type 2 spectra (Fig. 1) and the temperature-dependent trends (Fig. 2) are due to the cation ordering and disordering. Probably, the degree of the ordering affects the defect types and populations, and thus OH incorporation. This is the most likely explanation, although OH band assignment is not feasible with our data, and a general consensus has not been reached for the OH modes due to the chemical complexity in omphacite (Smyth et al., 1991; Katayama and Nakashima, 2003; Bromiley and Keppler, 2004; Koch-Müller et al., 2004). The linear increase of Abs_{3620}/Abs_{3450} of type 1 spectra with temperature probably reflects the gradual cation disorder and coupled OH incorporation. The disorder facilitates the OH incorporation, causing the 3620 cm^{-1} band, as seen by the temperature-enhanced intensity in type 1 spectra and the high intensity in type 2 spectra. Our data imply that the transition of the $P2/n$ to the $C2/c$ space group occurs at 750–800 °C at 1 GPa and 850–900 °C at 2 GPa. This resembles the results of previous work; e.g., 725 ± 20 °C at 1.5–1.8 GPa by X-ray diffraction analyses (Fleet et al., 1978) and 950–1050 °C at 2 GPa by Raman analyses (Katerinopoulou et al., 2008). The difference between these transition temperatures is likely related to different sample composition and methods for studying the disorder and temperature accuracy in the experiment; e.g., a type S thermocouple used in this study versus an empirical estimation by Fleet et al. (1978) and a type K thermocouple used by Katerinopoulou et al. (2008). Beyond the transition temperature, which is pressure dependent, the cations are disordered. This increases the anharmonicity in the lattice and produces the OH broadening and the poor relation of Abs_{3620}/Abs_{3450} with pressure or temperature; e.g., the Abs_{3620}/Abs_{3450} ratios of type 2 spectra are similar over the studied conditions (Figs. 2B and 2C).

OH IN OMPHACITE AS A PROXY FOR THERMAL CONDITIONS

The distinct type 1 and type 2 spectra of omphacite at different temperatures (Figs. 1 and 2) offer a potential proxy for inferring the thermal conditions of OH incorporation. Omphacite is usually found in massif eclogites exposed by tectonic uplift and xenolith eclogites entrained by kimberlites. The peak temperature of eclogite metamorphism is lower in massifs, mostly <800 °C, compared to xenoliths, ≥1000 °C. In this context, the OH groups of omphacite should be dominated by type 1 spectra in massif but type 2 spectra in xenolith eclogites. This is confirmed by examining the OH bands in available reports (Katayama and Nakashima, 2003; Koch-Müller et al., 2004; Sheng et al., 2007): type 1 spectra are commonly observed in omphacite of low-temperature origin (<800 °C), and type 2 spectra at ≥1000 °C (Fig. 3A). Our experimental data are thus in line with those of natural samples. We suggest that the OH patterns in omphacite can be used to infer whether they equilibrated at low or high temperature. This is helpful for understanding whether OH in omphacite was modified during exhumation. Hydrogen is a highly mobile element, and

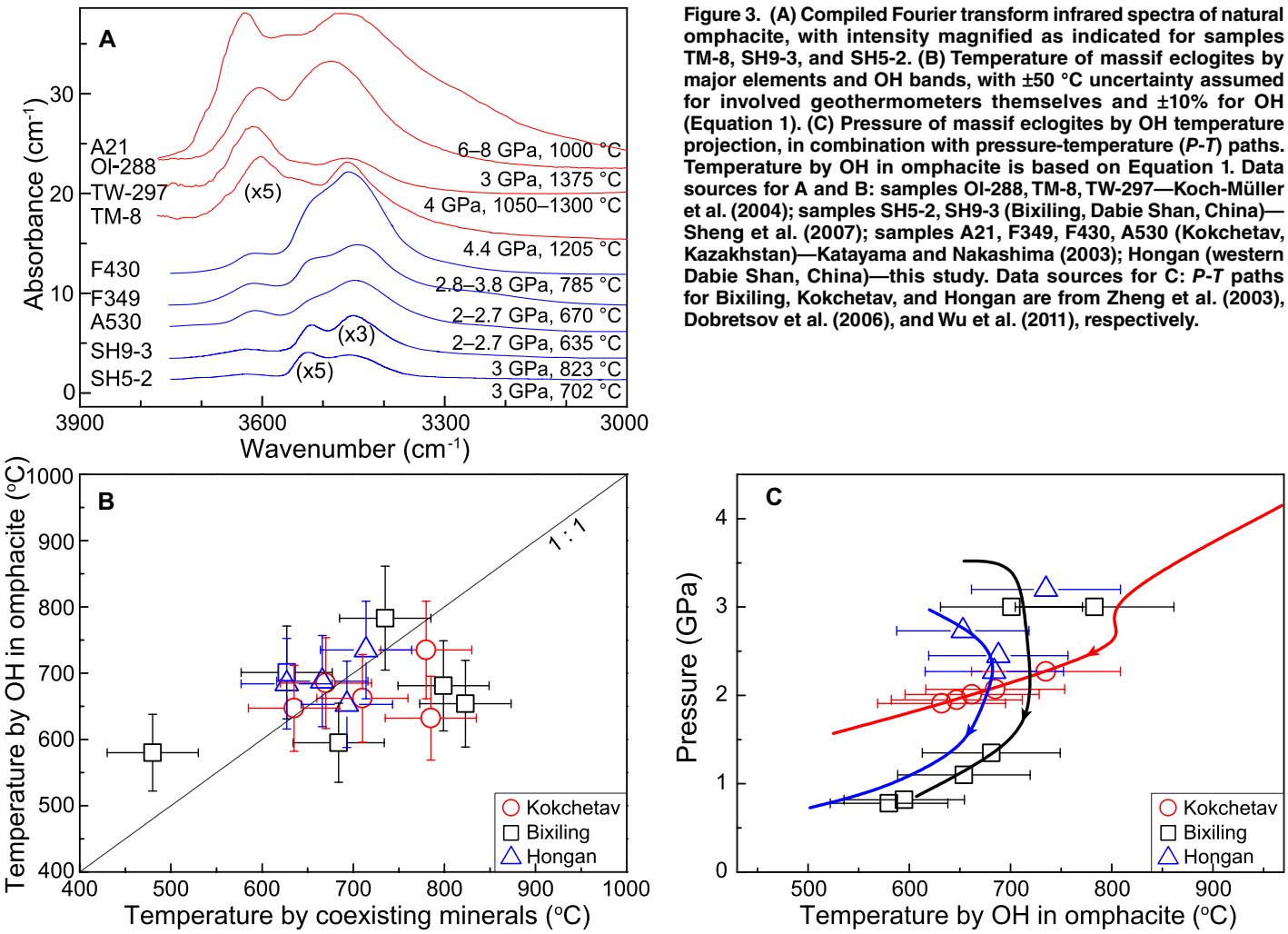

Figure 3. (A) Compiled Fourier transform infrared spectra of natural omphacite, with intensity magnified as indicated for samples TM-8, SH9-3, and SH5-2. (B) Temperature of massif eclogites by major elements and OH bands, with ±50 °C uncertainty assumed for involved geothermometers themselves and ±10% for OH (Equation 1). (C) Pressure of massif eclogites by OH temperature projection, in combination with pressure-temperature (*P-T*) paths. Temperature by OH in omphacite is based on Equation 1. Data sources for A and B: samples OI-288, TM-8, TW-297—Koch-Müller et al. (2004); samples SH5-2, SH9-3 (Bixiling, Dabie Shan, China)—Sheng et al. (2007); samples A21, F349, F430, A530 (Kokchetav, Kazakhstan)—Katayama and Nakashima (2003); Hongan (western Dabie Shan, China)—this study. Data sources for C: *P-T* paths for Bixiling, Kokchetav, and Hongan are from Zheng et al. (2003), Dobretsov et al. (2006), and Wu et al. (2011), respectively.

its initial information in the deep Earth can be partly or wholly reset by secondary processes; in contrast, major elements such as Mg, Al, and Fe are less mobile, and their equilibrium distribution is normally preserved and thus relevant for thermometry. The OH groups of omphacite in some xenolith eclogites equilibrated at >1000 °C show type 1 instead of type 2 spectra; e.g., sample SBB-1 of Smyth et al. (1991) and sample 2290 of Koch-Müller et al. (2004). OH in those samples may have been re-equilibrated rapidly at lower temperature while the major elements remained unmodified. However, most kimberlite eclogites ascended fast and cooled rapidly, so that the type 2 spectra of omphacite were retained.

The linear dependence of Abs_{3620}/Abs_{3450} of type 1 spectra on temperature (Fig. 2B) may be used to infer the temperature of OH equilibrium in natural omphacite, thus the thermal history of eclogites. We have tested this by estimating temperature with OH in omphacite and with major elements in coexisting omphacite and garnet. The samples are massif eclogites, with typical type 1 spectra in omphacite, from Bixiling in the eastern Dabie Shan (China) and Kokchetav (Kazakhstan) as reported previously (Katayama and Nakashima, 2003; Sheng et al., 2007) and Hongan in the western Dabie Shan (Table S3). The data are broadly consistent, mostly clustering around the 1:1 line in Figure 3B. The data scatter may be linked to (1) uncertainty of 50–150 °C in available geothermometers (Nakamura, 2009); (2) OH content determined by unpolarized analyses of limited grains in some samples, e.g., a single spectrum for each sample in Katayama and Nakashima (2003); and (3) OH re-equilibration after eclogite peak metamorphism. This provides a simple yet effective way to estimate the thermal state of eclogites. Especially, the high mobility of hydrogen and its sensitivity to fluids enable recording subtle information of rock evolution. Because OH incorporation can occur at any pressure during exhumation, water in natural omphacite, in combination with reported pressure-temperature (*P-T*) paths, allows establishment of the fluid-involved thermal evolution of massif eclogites. We refined fluid reactions of eclogites for Bixiling, Kokchetav, and Hongan by projecting OH-estimated temperature on the *P-T* paths of massif exhumation (Fig. 3C). This yielded a high-resolution fingerprint for the thermal conditions of eclogite history (while the peak major elements may have been mostly retained) and thus the thermal and tectonic evolution of crust overthrusting by continental collision.

Finally, we want to note that OH content in omphacite is also affected by crystal vacancies and composition, as shown for xenolith eclogites (Smyth et al., 1991; Koch-Müller et al., 2004). The compositional role in changing the temperature-related Abs_{3620}/Abs_{3450} trend (Fig. 2) has not been addressed in this study. The poor dependence of OH content in omphacite from massif eclogites on crystal vacancies and composition (Sheng et al., 2007), compared to that from xenolith eclogites, due probably to their different origins (Jacob, 2004) and mineral defects, suggests, however, that the effect of composition on Equation 1 may not be significant. Further experiments on omphacite of different compositions may shed new light onto this issue.

ACKNOWLEDGMENTS

We thank Monica Koch-Müller for supplying the spectral data of omphacite in xenolith eclogites, and Mike Jollands, Bertrand Moine, and one anonymous

reviewer for helpful comments. This study was supported by National Science Foundation of China (grant 41725008) and the National Key R&D Program of China (grant 2018YFA0702704).

REFERENCES CITED

Bromiley, G.D., and Keppler, H., 2004, An experimental investigation of hydroxyl solubility in jadeite and Na-rich clinopyroxenes: Contributions to Mineralogy and Petrology, v. 147, p. 189–200, https://doi.org/10.1007/s00410-003-0551-1.

Bromiley, G.D., Keppler, H., McCammon, C., Bromiley, F.A., and Jacobsen, S.D., 2004, Hydrogen solubility and speciation in natural, gem-quality chromian diopside: American Mineralogist, v. 89, p. 941–949, https://doi.org/10.2138/am-2004-0703.

Costa, F., and Chakraborty, S., 2008, The effect of water on Si and O diffusion rates in olivine and implications for transport properties and processes in the upper mantle: Physics of the Earth and Planetary Interiors, v. 166, p. 11–29, https://doi.org/10.1016/j.pepi.2007.10.006.

Dobretsov, N.L., Buslov, M.M., Zhimulev, F.I., Travin, A.V., and Zayachkovsky, A.A., 2006, Vendian–Early Ordovician geodynamic evolution and model for exhumation of ultrahigh- and high-pressure rocks from the Kokchetav subduction-collision zone (northern Kazakhstan): Russian Geology and Geophysics, v. 47, p. 424–440.

Fleet, M.E., Herzberg, C.T., Bancroft, G.M., and Aldridge, L.P., 1978, Omphacite studies: I, The $P2/n \rightarrow C2/c$ transformation: American Mineralogist, v. 63, p. 1100–1106.

Gaetani, G.A., and Grove, T.L., 1998, The influence of water on melting of mantle peridotite: Contributions to Mineralogy and Petrology, v. 131, p. 323–346, https://doi.org/10.1007/s004100050396.

Hier-Majumder, S., Anderson, I.M., and Kohlstedt, D.L., 2005, Influence of protons on Fe-Mg interdiffusion in olivine: Journal of Geophysical Research, v. 110, B02202, https://doi.org/10.1029/2004JB003292.

Hirose, K., and Kawamoto, T., 1995, Hydrous partial melting of lherzolite at 1 GPa: The effect of H_2O on the genesis of basaltic magmas: Earth and Planetary Science Letters, v. 133, p. 463–473, https://doi.org/10.1016/0012-821X(95)00096-U.

Jacob, D.E., 2004, Nature and origin of eclogite xenoliths from kimberlites: Lithos, v. 77, p. 295–316, https://doi.org/10.1016/j.lithos.2004.03.038.

Karato, S., 1990, The role of hydrogen in the electrical conductivity of the upper mantle: Nature, v. 347, p. 272–273, https://doi.org/10.1038/347272a0.

Katayama, I., and Nakashima, S., 2003, Hydroxyl in clinopyroxene from the deep subducted crust: Evidence for H_2O transport into mantle: American Mineralogist, v. 88, p. 229–234, https://doi.org/10.2138/am-2003-0126.

Katayama, I., Nakashima, S., and Yurimoto, H., 2006, Water content in natural eclogite and implication for water transport into the deep upper mantle: Lithos, v. 86, p. 245–259, https://doi.org/10.1016/j.lithos.2005.06.006.

Katerinopoulou, A., Musso, M., and Amthauer, G., 2008, A Raman spectroscopic study of the phase transition in omphacite: Vibrational Spectroscopy, v. 48, p. 163–167, https://doi.org/10.1016/j.vibspec.2007.12.015.

Koch-Müller, M., Matsyuk, S.S., and Wirth, R., 2004, Hydroxyl in omphacites and omphacitic clinopyroxenes of upper mantle to lower crustal origin beneath the Siberian platform: American Mineralogist, v. 89, p. 921–931, https://doi.org/10.2138/am-2004-0701.

Kohlstedt, D.L., Keppler, H., and Rubie, D.C., 1996, Solubility of water in the α, β, and γ phases of $(Mg,Fe)_2SiO_4$: Contributions to Mineralogy and Petrology, v. 123, p. 345–357, https://doi.org/10.1007/s004100050161.

Kovács, I., Hermann, J., O'Neil, H.S.C., Gerald, J.F., Sambridge, M., and Horváth, G., 2008, Quantitative absorbance spectroscopy with unpolarized light: Part II. Experimental evaluation and development of a protocol for quantitative analysis of mineral IR spectra: American Mineralogist, v. 93, p. 765–778, https://doi.org/10.2138/am.2008.2656.

Liu, H., and Yang, X., 2020, Solubility of hydroxyl groups in pyroxenes: Effect of oxygen fugacity at 0.2–3 GPa and 800–1200°C: Geochimica et Cosmochimica Acta, v. 286, p. 355–379, https://doi.org/10.1016/j.gca.2020.07.034.

Liu, H., Zhang, K., Ingrin, J., and Yang, X., 2021, Electrical conductivity of omphacite and garnet indicates limited deep water recycling by crust subduction: Earth and Planetary Science Letters, v. 559, 116784, https://doi.org/10.1016/j.epsl.2021.116784.

Mackwell, S.J., Kohlstedt, D.L., and Paterson, M.S., 1985, The role of water in the deformation of olivine single crystals: Journal of Geophysical Research, v. 90, p. 11,319–11,333, https://doi.org/10.1029/JB090iB13p11319.

Mei, S., and Kohlstedt, D.L., 2000, Influence of water on plastic deformation of olivine aggregates: 1. Diffusion creep regime: Journal of Geophysical Research, v. 105, p. 21,457–21,469, https://doi.org/10.1029/2000JB900179.

Moine, B.N., Bolfan-Casanova, N., Radu, I.B., Ionov, D.A., Costin, G., Korsakov, A.V., Golovin, A.V., Oleinikov, O.B., Deloule, E., and Cottin, J.Y., 2020, Molecular hydrogen in minerals as a clue to interpret δD variations in the mantle: Nature Communications, v. 11, 3604, https://doi.org/10.1038/s41467-020-17442-8.

Nakamura, D., 2009, A new formulation of garnet–clinopyroxene geothermometer based on accumulation and statistical analysis of a large experimental data set: Journal of Metamorphic Geology, v. 27, p. 495–508, https://doi.org/10.1111/j.1525-1314.2009.00828.x.

Schmädicke, E., and Gose, J., 2017, Water transport by subduction: Clues from garnet of Erzgebirge UHP eclogite: American Mineralogist, v. 102, p. 975–986, https://doi.org/10.2138/am-2017-5920.

Schmidt, M.W., and Poli, S., 2014, Devolatilization during subduction, *in* Rudnick, R.L., ed., Treatise on Geochemistry (second edition), Volume 4: The Crust: Amsterdam, Elsevier Science, p. 669–701, https://doi.org/10.1016/B978-0-08-095975-7.00321-1.

Sheng, Y.-M., Xia, Q.-K., Dallai, L., Yang, X.-Z., and Hao, Y.-T., 2007, H_2O contents and D/H ratios of nominally anhydrous minerals from ultrahigh-pressure eclogites of the Dabie orogen, eastern China: Geochimica et Cosmochimica Acta, v. 71, p. 2079–2103, https://doi.org/10.1016/j.gca.2007.01.018.

Skogby, H., Bell, D.R., and Rossman, G.R., 1990, Hydroxide in pyroxene: Variations in the natural environment: American Mineralogist, v. 75, p. 764–774.

Smyth, J.R., Bell, D.R., and Rossman, G.R., 1991, Incorporation of hydroxyl in upper-mantle clinopyroxenes: Nature, v. 351, p. 732–735, https://doi.org/10.1038/351732a0.

Wu, Y., Gao, S., Liu, X., Wang, J., Peng, M., Gong, H., and Yuan, H., 2011, Two-stage exhumation of ultrahigh-pressure metamorphic rocks from the western Dabie Orogen, central China: The Journal of Geology, v. 119, p. 15–31, https://doi.org/10.1086/657259.

Yang, X., 2015, OH solubility in olivine in the peridotite-COH system under reducing conditions and implications for water storage and hydrous melting in the reducing upper mantle: Earth and Planetary Science Letters, v. 432, p. 199–209, https://doi.org/10.1016/j.epsl.2015.10.014.

Yang, X., 2016, Effect of oxygen fugacity on OH dissolution in olivine under peridotite-saturated conditions: An experimental study at 1.5–7 GPa and 1100–1300 °C: Geochimica et Cosmochimica Acta, v. 173, p. 319–336, https://doi.org/10.1016/j.gca.2015.11.007.

Yang, X., and McCammon, C., 2012, Fe^{3+}-rich augite and high electrical conductivity in the deep lithosphere: Geology, v. 40, p. 131–134, https://doi.org/10.1130/G32725.1.

Yang, X., Keppler, H., McCammon, C., Ni, H., Xia, Q., and Fan, Q., 2011, The effect of water on the electrical conductivity of lower crustal clinopyroxene: Journal of Geophysical Research, v. 116, B04208, https://doi.org/10.1029/2010JB008010.

Yang, X., Keppler, H., and Li, Y., 2016, Molecular hydrogen in mantle minerals: Geochemical Perspectives Letters, v. 2, p. 160–168, https://doi.org/10.7185/geochemlet.1616.

Zhang, B., Yoshino, T., Wu, X., Matsuzaki, T., Shan, S., and Katsura, T., 2012, Electrical conductivity of enstatite as a function of water content: Implications for the electrical structure in the upper mantle: Earth and Planetary Science Letters, v. 357–358, p. 11–20, https://doi.org/10.1016/j.epsl.2012.09.020.

Zheng, Y.-F., Fu, B., Gong, B., and Li, L., 2003, Stable isotope geochemistry of ultrahigh pressure metamorphic rocks from the Dabie-Sulu orogen in China: Implications for geodynamics and fluid regime: Earth-Science Reviews, v. 62, p. 105–161, https://doi.org/10.1016/S0012-8252(02)00133-2.

Printed in USA